

RESEARCH ARTICLE

The earliest stage of Izu rear-arc volcanism revealed by drilling at Site U1437, International Ocean Discovery Program Expedition 350

Tomoki Sato¹  | Takashi Miyazaki¹  | Yoshihiko Tamura¹  | James B. Gill²  |
Martin Jutzeler³  | Ryoko Senda⁴ | Jun-Ichi Kimura¹

¹Research Institute for Marine Geodynamics, Japan Agency for Marine-Earth Science and Technology, Yokosuka, Japan

²Department of Earth and Planetary Science, University of California Santa Cruz, Santa Cruz, California, USA

³School of Natural Sciences and Centre for Ore Deposit and Earth Sciences, University of Tasmania, Hobart, Tasmania, Australia

⁴Faculty of Social and Cultural Studies, Kyushu University, Fukuoka, Japan

Correspondence

Yoshihiko Tamura, 2-15 Natsushima-cho, Yokosuka, 237-0061 Japan.
Email: tamuray@jamstec.go.jp

Funding information

Japan Society for the Promotion of Science, Grant/Award Numbers: KAKENHI Grant Numbers JP16H02742, JP16H06347, JP17K05686, and JP17H02987; Natural Environment Research Council, Grant/Award Number: grant NE/M005224/1

Abstract

The International Ocean Discovery Program Expedition 350 drilled between two Izu rear-arc seamount chains at Site U1437 and recovered the first complete succession of rear-arc rocks. The drilling reached 1806.5 m below seafloor. In situ hyaloclastites, which had erupted before the rear-arc seamounts came into existence at this site, were recovered in the deepest part of the hole (~15–16 Ma). Here it is found that the composition of the oldest rocks recovered does not have rear-arc seamount chain geochemical signatures, but instead shows affinities with volcanic front or some of the extensional zone basalts between the present volcanic front and the rear-arc seamount chains. It is suggested that following the opening of the Shikoku back-arc Basin, Site U1437 was a volcanic front or a rifting zone just behind the volcanic front, and was followed at ~9 Ma by the start of rear-arc seamount chains volcanism. This geochemical change records variations in the subduction components with time, which might have followed eastward moving of hot fingers in the mantle wedge and deepening of the subducting slab below Site U1437 after the cessation of Shikoku back-arc Basin opening.

KEYWORDS

andesite, basalt, IODP, Izu-Ogasawara arc, Miocene, oceanic arc, Pacific plate, rear-arc, slab depth, subduction

1 | INTRODUCTION

The Izu arc (Figure 1a) is a classic oceanic arc characterized by two types of basalt magmas (Tamura et al., 2005, 2007) and bimodal volcanism that produces basalt and rhyolite magmas (Shukuno et al., 2006; Tamura & Tatsumi, 2002), and magma types have been correlated to crustal structures (Kodaira, Sato, Takahashi, Ito, et al., 2007; Kodaira, Sato, Takahashi, Miura, et al., 2007; Tamura et al., 2009; Tamura, Sato, Fujiwara, Kodaira, & Nichols, 2016). The Izu arc is also characterized by Miocene rear-arc seamount chains developed at high angle to the

arc (Ishizuka, Uto, & Yuasa, 2003; Kodaira et al., 2008; Figure 1b). Despite extensive research carried out in the Izu rear-arc through multiple dredging and remotely operated vehicle sampling expeditions, its magmatic history is poorly known, and it is unclear how and when the Izu rear-arc acquired its continental crust-like composition in terms of trace elements, such as light rare earth element (LREE)-enriched patterns (Tamura et al., 2015b). The rear-arc seamount chain volcanism was active from 12 to 3 Ma (Ishizuka, Uto, & Yuasa, 2003) and one older andesite (17 Ma) has been found in the westernmost Kan'ei chain (Ishizuka, Uto, & Yuasa, 2003).

This is an open access article under the terms of the Creative Commons Attribution License, which permits use, distribution and reproduction in any medium, provided the original work is properly cited.

© 2020 The Authors. *Island Arc* Published by John Wiley & Sons Australia, Ltd

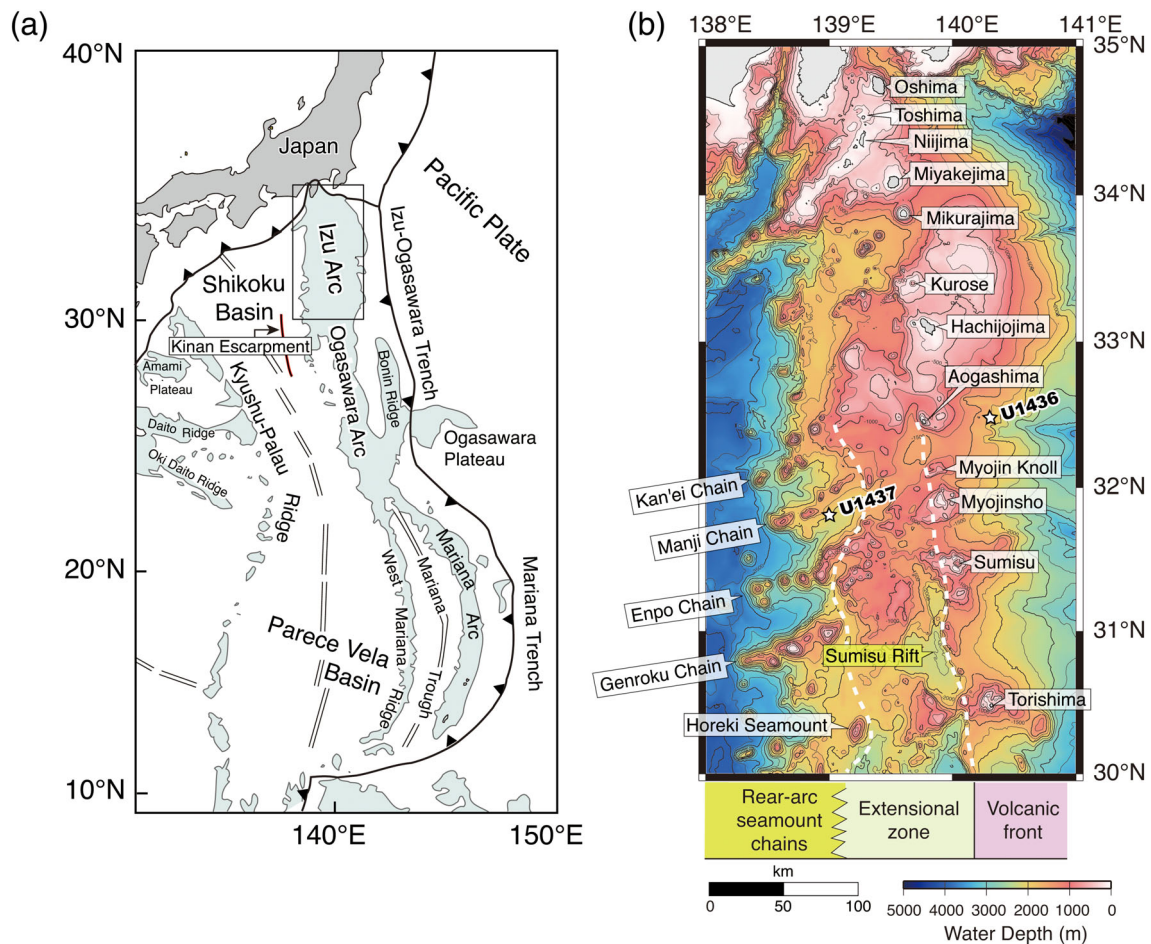


FIGURE 1 (a) The structure of the Izu-Ogasawara-Mariana arc system (Taylor, 1992). Double lines indicate spreading centers, active in the Mariana Trough and relic in the Shikoku and Parece Vela Basins. The Izu-Ogasawara, West Mariana, and Mariana arcs are outlined by the 3 km bathymetric contour and other basins and ridges are outlined by the 4 km contour. (b) Seafloor bathymetry of the northern Izu-Ogasawara arc. The Quaternary arc-front volcanoes (Oshima, Toshima, Miyakejima, Mikurajima, Kurose, Hachijojima, Aogashima, Myojin Knoll, Myojinsho, Sumisu, Torishima) and Pliocene–Miocene rear-arc seamount chains (Kan'e, Manji, Enpo, and Genroku Chains and Horeki Seamount), and Sumisu rift in the extensional zone are shown. The summits of many frontal volcanoes have grown above sea level to form the Izu-Ogasawara (Bonin) islands. White stars, the locations of IODP EXP350 Sites U1436 and U1437; dashed lines, eastern and western margins of extensional zone

Site U1437 of the International Ocean Discovery Program (IODP) Expedition 350 is located between the Manji and Enpo rear-arc seamount chains. At this site, the recovery of an *in situ* volcanic succession subsequently covered by > 1400 m of sediments provides the first information on the magmatism before the formation of the rear-arc seamount chains. In this study, we present whole rock chemical compositions collected from the deepest part of the drilling site, which we interpret as not derived from the Izu rear-arc volcanism in its current form. This study thus reveals important information on the previous stage of Izu rear-arc volcanism and on the complexity of arc and rear-arc magmatism.

1.1 | Background

The Izu-Ogasawara (or Izu-Bonin) arc crust, south of Honshu Island, Japan, has been formed by arc magmatism related to the subduction of the Pacific plate beneath the Philippine Sea plate. It is an excellent

example of the possible formation of juvenile continental crust in an intra-oceanic convergent margin system (Kodaira et al., 2008; Suyehrio, Takahashi, Arie, & Yokoi, 1996; Tamura et al., 2016; Tamura, Ishizuka, Sato, & Nichols, 2019). Figure 1b shows the present Izu arc system, which consists of three types of volcanic environments: (i) Quaternary arc-front volcanoes that are parallel to the Izu-Ogasawara trench (volcanic front); (ii) Miocene–Pliocene rear-arc seamount chains consisting of volcanoes lying at a high angle (60–70°) to the arc; and (iii) < 2.8 Ma (Ishizuka, Uto, & Yuasa, 2003; Ishizuka, Uto, Yuasa, & Hochstaedter, 1998) bimodal rift-type volcanoes in the extensional zone between the volcanic front and rear-arc seamount chains.

The rear-arc seamount chains have been interpreted to have formed after cessation of seafloor spreading in the Shikoku back-arc Basin at ~ 15 Ma (Okino, Ohara, Kasuga, & Kato, 1999). The seamount chains show a trend toward becoming younger from west to east (Ishizuka, Uto, & Yuasa, 2003). The formation of the seamount

chains might be related to compression caused by collision between the southwest Japan and Izu arcs associated with the Japan Sea opening (Bandy & Hilde, 1983; Karig & Moore, 1975), or they might overlie Shikoku Basin transform faults (Yamazaki & Yuasa, 1998). Kodaira et al. (2008) showed that the north–south spacing of rear-arc volcanoes is not linked to the underlying undulating thick and thin crustal structure, suggesting that thick parts of rear-arc crust had been produced in Oligocene before the formation of the Shikoku Basin (25–15 Ma). Another possible hypothesis is that the seamount chains overlie hot regions in the mantle wedge, such as the hot fingers proposed for northeast Japan that intruded into the mantle wedge from west to east (Honda, Yoshida, & Aoike, 2007; Tamura, Tatsumi, Zhao, Kido, & Shukuno, 2002).

IODP Expedition Site U1437 is located in a volcano-bounded basin between the Manji and Enpo rear-arc seamount chains at a

depth of 2117 m below sea level, and ~ 90 km west of the arc-front volcano Myojinsho (Figure 1b). Figure 2 shows the age-depth diagram of Site U1437. A seismic reflection profile, showing the nature of the studied units, is presented in Yamashita, Takahashi, Tamura, Miura, and Kodaira (2018). Drilling at Site U1437 reached 1806.5 m below seafloor (mbsf). During the expedition, the recovered rocks were divided into seven lithostratigraphic units from Unit I to Unit VII and one igneous unit (Igneous Unit 1) within lithostratigraphic Unit VI that consists of a peperitic rhyolite intrusion (Tamura et al., 2015b). Overlying volcanoclastic sediments (Units I to Unit VI) were derived from nearby rear-arc and/or distal volcanic front volcanoes (Tamura et al., 2015b ; Gill et al., 2018). Magnetic stratigraphy derived from polarity reversals was used down to 1300 mbsf at the base of Unit V, suggesting ~ 9 Ma (Tamura et al., 2015b).

Secondary ion mass spectrometry U–Pb zircon ages obtained from Igneous Unit 1 and Unit VII are (13.9 ± 0.2) Ma and (15.4 ± 0.8) Ma, respectively (Schmitt et al., 2018). Unit VII records the oldest magmatism discovered during Expedition 350, and it occurred after the end of the adjacent Shikoku back-arc Basin spreading.

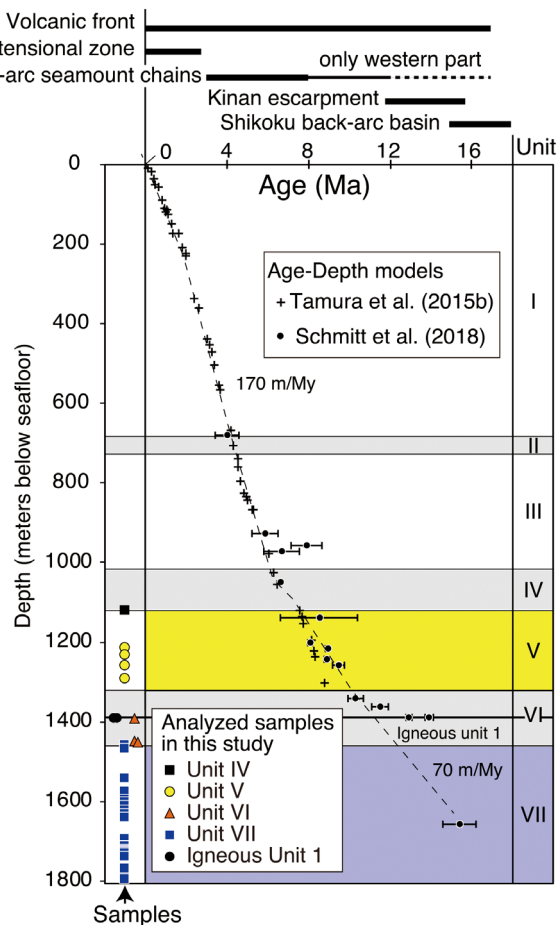


FIGURE 2 Lithostratigraphic units and age-depth plot of Site U1437. Lithostratigraphic unit depths (Units I to VII and Igneous Unit 1) are from Tamura et al. (2015b). Plus signs show biostratigraphic and paleomagnetic age data from Tamura et al. (2015b). Filled circles show $^{40}\text{Ar}/^{39}\text{Ar}$ and U–Pb zircon age data from Schmitt et al. (2018). Dashed lines show sedimentation rates for different times, ranging from ~ 170 m/my in Unit I to ~ 70 m/my in Units V, VI, and VII. The bars on the top of this figure show the active period of each volcanism. The depths of the samples of this study are shown on the left side of the figure

2 | MATERIAL AND METHOD

2.1 | Provenance of Unit VII

Unit VII is the deepest portion of Site U1437 from 1460 to 1806 mbsf (Figure 2), and consists of ~ 350 m of relatively homogeneous, coarse-grained, hyaloclastite units. Most hyaloclastites have framework-supported lapilli-size clasts with a wide range in vesicularity (0–80 vol %) and crystallinity (glassy to porphyritic).

Parts of Unit VII are thick monomictic breccia interpreted to be hyaloclastite deposits showing macroscopic textural evidence of quench fragmentation (e.g., quenched concave margins, and emplacement at high temperature). In the lower part of Unit VII, Core Section 70R2 (1721 mbsf) is made of metric domains of very angular, moderately vesicular lava surrounded by jigsaw fit breccia of the same composition, in which alteration pipes occur, all attesting to in situ hyaloclastite. Alteration pipes in Core Section 68R3 (1703 mbsf) suggest another in situ facies. Core Section 59R2 (1623 mbsf) contains numerous coarse, poorly vesicular lava clasts with delicate quench margins, and may also represent in situ facies. Cores 42R to 54R consist of a > 100 m-thick, black, framework-supported, hyaloclastite breccia that broadly grades from being dense clast-dominated to pumice clast-dominated. With the exception of some hydrothermally altered red clasts, the breccia is very homogeneous in type of components and grain size, and is considered monomictic overall. Most of the unit is nonstratified, although its top includes normally graded beds. The presence of stratification attests to at least partial resedimentation, but the overall homogeneity indicates that it is a proximal hyaloclastite facies, with minimal resedimentation involved. These lines of evidence suggest that these are near-vent facies and, therefore, representing magmas emplaced at or at close distance from the drill site.

TABLE 1 Whole rock major and trace element compositions of samples from Units IV–VII of Hole U1437E

Unit:	Unit IV	Unit V				Unit VI	
Sample ID:	6R3W-100/102	17R2W-125/127	19R2W-0/2	21R6W-43/44	25R3W-54/56	35R3W-60/62	41R2W-19/21
Depth (mbsf):	1119.90	1215.99	1234.03	1259.88	1293.87	1391.63	1448.20
Lithology:	Lapilli tuff	Lapilli stone	Lapilli tuff	Lapilli tuff	Lapilli tuff	Lapilli	Lapilli
Host rock:	–	–	–	–	–	Lapilli stone	Tuff breccia
Major element (wt%) by XRF							
SiO ₂	54.41	52.38	52.04	52.21	57.93	71.62	51.13
TiO ₂	0.99	1.21	0.86	1.07	0.71	0.25	1.03
Al ₂ O ₃	17.00	18.81	17.61	17.72	18.96	15.52	19.67
Fe ₂ O ₃	11.66	10.27	10.42	11.23	8.95	1.94	8.90
MnO	0.18	0.13	0.13	0.16	0.26	0.04	0.23
MgO	5.03	4.95	5.00	4.25	2.09	0.22	4.22
CaO	7.46	8.50	9.30	8.78	2.97	2.06	9.85
Na ₂ O	1.49	2.85	2.80	2.92	7.94	5.46	3.58
K ₂ O	1.63	0.48	1.24	1.37	0.44	2.64	0.88
P ₂ O ₅	0.11	0.16	0.21	0.23	0.14	0.06	0.20
Total	99.95	99.74	99.60	99.93	100.37	99.82	99.69
LOI	8.10	5.95	11.29	5.12	7.33	2.32	3.42
Trace element (ppm) by XRF							
Ba	237.3	114.1	–	133.7	50.0	267.2	64.6
Ni	13.2	27.9	–	17.4	6.4	n.d.	22.4
Cu	126.3	47.6	–	41.7	41.2	2.9	48.9
Zn	111.8	102.5	–	109.5	137.8	21.6	95.3
Pb	2.9	2.8	–	3.8	6.5	2.1	2.2
Rb	14.0	6.6	–	8.2	5.4	24.2	6.7
Sr	507.4	373.0	–	324.8	67.2	121.8	267.0
Y	24.4	26.6	–	30.3	37.8	11.1	36.5
Zr	57.1	113.7	–	88.3	76.2	107.1	94.3
Nb	(0.7)	(3.2)	–	(2.5)	n.d.	(0.9)	(1.5)
Cr	13.8	21.6	–	16.6	8.6	5.5	64.4
V	337.8	295.2	–	316.3	88.0	26.6	311.1
Trace element (ppm) by ICP-MS							
Sc	–	–	24.7	29.6	–	–	–
Co	–	–	33.4	29.0	–	–	–
Ni	–	–	27.8	16.2	–	–	–
Cu	–	–	42.9	38.6	–	–	–
Rb	–	–	10.92	7.12	–	–	–
Sr	–	–	359	316	–	–	–
Y	–	–	23.3	29.8	–	–	–
Zr	–	–	65.4	82.7	–	–	–
Nb	–	–	2.47	2.44	–	–	–
Cs	–	–	0.21	0.18	–	–	–
Ba	–	–	156	133	–	–	–
La	–	–	7.33	7.87	–	–	–
Ce	–	–	17.4	20.4	–	–	–
Pr	–	–	2.39	3.01	–	–	–
Nd	–	–	10.8	14.3	–	–	–

(Continues)

TABLE 1 (Continued)

Unit:	Unit IV	Unit V				Unit VI	
Sample ID:	6R3W-100/102	17R2W-125/127	19R2W-0/2	21R6W-43/44	25R3W-54/56	35R3W-60/62	41R2W-19/21
Depth (mbsf):	1119.90	1215.99	1234.03	1259.88	1293.87	1391.63	1448.20
Lithology:	Lapilli tuff	Lapilli stone	Lapilli tuff	Lapilli tuff	Lapilli tuff	Lapilli	Lapilli
Host rock:	—	—	—	—	—	Lapilli stone	Tuff breccia
Sm	—	—	2.85	3.96	—	—	—
Eu	—	—	0.971	1.22	—	—	—
Gd	—	—	3.33	4.66	—	—	—
Tb	—	—	0.573	0.790	—	—	—
Dy	—	—	3.83	5.14	—	—	—
Ho	—	—	0.856	1.12	—	—	—
Er	—	—	2.65	3.40	—	—	—
Tm	—	—	0.386	0.500	—	—	—
Yb	—	—	2.51	3.38	—	—	—
Lu	—	—	0.386	0.521	—	—	—
Hf	—	—	1.79	2.38	—	—	—
Ta	—	—	0.189	0.169	—	—	—
Tl	—	—	0.192	0.074	—	—	—
Pb	—	—	9.24	5.03	—	—	—
Th	—	—	1.410	1.300	—	—	—
U	—	—	0.528	0.519	—	—	—

Unit:	Unit VI	Unit VII					
Sample ID:	41R4W-129/133	42R4W-106/112	43R2W-98/101	51R1W-40/42	54R2W-87/89	56R5W-128/130	57R1W-58/60
Depth (mbsf):	1452.11	1461.68	1468.27	1544.21	1575.38	1598.54	1602.79
Lithology:	Lapilli tuff	Lapilli tuff	Volcanic block	Volcanic block	Lapilli	Volcanic block	Volcanic block
Host rock:	—	—	Lapilli stone	Lapilli tuff	Lapilli tuff	Lapilli tuff	Lapilli stone

Major element (wt%) by XRF

SiO ₂	53.22	50.50	55.55	49.94	56.37	49.06	52.95
TiO ₂	0.97	0.91	0.75	0.93	1.29	0.96	0.88
Al ₂ O ₃	18.22	22.16	19.01	19.98	19.24	21.79	19.31
Fe ₂ O ₃	10.42	9.53	5.60	9.12	7.08	9.27	7.87
MnO	0.23	0.14	0.19	0.22	0.18	0.18	0.17
MgO	7.24	5.96	2.83	5.69	3.39	3.92	3.94
CaO	7.65	9.80	12.40	11.23	6.86	11.83	9.64
Na ₂ O	1.24	1.27	2.03	2.64	3.70	2.96	4.53
K ₂ O	0.72	0.10	0.23	0.11	1.53	0.20	0.39
P ₂ O ₅	0.16	0.10	1.24	0.16	0.31	0.15	0.14
Total	100.07	100.45	99.82	100.03	99.93	100.31	99.82
LOI	6.08	5.20	3.69	2.73	11.53	2.50	1.41

Trace element (ppm) by XRF

Ba	n.d.	n.d.	37.8	n.d.	—	26.2	74.9
Ni	40.9	12.2	18.9	46.4	—	32.1	50.7
Cu	118.5	62.4	69.4	64.5	—	89.8	40.5
Zn	108.2	85.0	151.0	90.6	—	90.9	129.1

(Continues)

TABLE 1 (Continued)

Unit:	Unit VI	Unit VII					
	41R4W- 129/133 Depth (mbsf): 1452.11	42R4W- 106/112 1461.68	43R2W- 98/101 1468.27	51R1W- 40/42 1544.21 Volcanic block	54R2W- 87/89 1575.38	56R5W- 128/130 1598.54	57R1W-58/60 1602.79
Lithology: Host rock:	Lapilli tuff –	Lapilli tuff –	Volcanic block Lapilli stone	Volcanic block Lapilli tuff	Lapilli Lapilli tuff	Volcanic block Lapilli tuff	Volcanic block Lapilli stone
Pb	6.4	2.1	2.6	n.d.	–	1.9	3.1
Rb	8.5	2.3	2.4	1.9	–	2.9	5.1
Sr	161.2	208.0	249.1	254.3	–	274.0	223.3
Y	25.2	19.0	34.0	27.7	–	21.5	26.7
Zr	63.2	52.5	35.9	79.4	–	54.0	77.4
Nb	(0.7)	(1.0)	(0.6)	(0.9)	–	(0.5)	(1.0)
Cr	53.4	16.7	75.5	112.3	–	85.4	159.0
V	283.0	342.0	261.2	292.7	–	349.9	275.4

Trace element (ppm) by ICP-MS

Sc	–	22.3	–	–	–	–	–
Co	–	19.6	–	–	–	–	–
Ni	–	9.64	–	–	–	–	–
Cu	–	57.4	–	–	–	–	–
Rb	–	1.34	–	–	–	–	–
Sr	–	190	–	–	–	–	–
Y	–	17.2	–	–	–	–	–
Zr	–	49.6	–	–	–	–	–
Nb	–	0.63	–	–	–	–	–
Cs	–	0.06	–	–	–	–	–
Ba	–	13.3	–	–	–	–	–
La	–	2.94	–	–	–	–	–
Ce	–	8.07	–	–	–	–	–
Pr	–	1.30	–	–	–	–	–
Nd	–	6.74	–	–	–	–	–
Sm	–	2.13	–	–	–	–	–
Eu	–	0.791	–	–	–	–	–
Gd	–	2.77	–	–	–	–	–
Tb	–	0.486	–	–	–	–	–
Dy	–	3.22	–	–	–	–	–
Ho	–	0.692	–	–	–	–	–
Er	–	2.08	–	–	–	–	–
Tm	–	0.303	–	–	–	–	–
Yb	–	2.00	–	–	–	–	–
Lu	–	0.303	–	–	–	–	–
Hf	–	1.49	–	–	–	–	–
Ta	–	0.043	–	–	–	–	–
Tl	–	0.015	–	–	–	–	–
Pb	–	1.88	–	–	–	–	–
Th	–	0.326	–	–	–	–	–
U	–	0.222	–	–	–	–	–

Unit:	Unit VII						
Sample ID:	57R1W-71/75	58R1W-34/36	58R2W-36/38	59R2W-60/64	60R2W-60/66	61R1W-10/14	66R4W-101/103
Depth (mbsf):	1603.10	1612.25	1613.70	1623.68	1633.42	1641.22	1695.05
Lithology:	Lapilli	Volcanic block	Volcanic block	Lapilli	Lapilli	Lapilli tuff	Volcanic block Tuff breccia and lapilli tuff
Host rock:	Lapilli stone	Tuff breccia	Tuff breccia	Lapilli tuff	Tuff breccia	-	

Major element (wt%) by XRF

SiO ₂	52.04	50.61	49.76	52.15	52.24	51.37	52.86
TiO ₂	1.13	1.05	0.88	1.06	1.14	0.98	1.10
Al ₂ O ₃	19.75	20.30	20.33	19.02	17.24	19.97	19.37
Fe ₂ O ₃	8.72	9.08	9.96	10.50	11.70	10.43	8.72
MnO	0.15	0.14	0.20	0.31	0.32	0.11	0.25
MgO	3.95	3.90	4.59	3.70	4.83	6.78	4.69
CaO	9.50	10.76	11.87	8.17	7.83	9.27	8.06
Na ₂ O	3.93	3.46	2.38	4.38	3.10	1.36	4.50
K ₂ O	0.69	0.47	0.23	0.60	1.36	0.12	0.62
P ₂ O ₅	0.25	0.18	0.12	0.27	0.46	0.08	0.25
Total	100.10	99.94	100.30	100.16	100.21	100.46	100.43
LOI	3.92	3.05	1.30	1.95	2.14	4.30	1.88

Trace element (ppm) by XRF

Ba	96.0	77.5	38.5	223.7	81.4	n.d.	113.8
Ni	21.9	49.6	31.5	17.3	10.7	18.3	12.6
Cu	85.3	35.6	54.8	78	57.6	57.3	60.0
Zn	110.3	82.6	77	108	175.9	87.7	100.3
Pb	2.0	2.4	1.9	1.6	2.4	2.1	3.3
Rb	7.2	4.9	2.0	6.6	10.1	3.2	7.9
Sr	275.7	297.0	268.8	278	219	219.7	283.1
Y	28.9	22.9	19.1	32	70.8	18.1	34.5
Zr	70.8	64.8	49.7	68.6	74	60.2	92.9
Nb	(1.2)	(1.2)	(0.8)	(1)	(1)	(0.9)	(1.3)
Cr	73.8	107.4	76.1	17.2	5.1	41.1	24.1
V	333.7	362.6	337.9	361.4	389.1	360.4	277.8

Trace element (ppm) by ICP-MS

Sc	—	—	30.4	—	32.1	—	—
Co	—	—	27.6	—	20.0	—	—
Ni	—	—	31.4	—	8.35	—	—
Cu	—	—	50.7	—	56.1	—	—
Rb	—	—	1.15	—	8.92	—	—
Sr	—	—	260	—	211	—	—
Y	—	—	18.1	—	69.2	—	—
Zr	—	—	49.7	—	75.2	—	—
Nb	—	—	0.63	—	1.02	—	—
Cs	—	—	0.02	—	0.08	—	—
Ba	—	—	48.5	—	95.4	—	—
La	—	—	3.13	—	11.40	—	—
Ce	—	—	8.50	—	26.8	—	—

(Continues)

TABLE 1 (Continued)

Unit:	Unit VII						
Sample ID:	57R1W-71/75	58R1W-34/36	58R2W-36/38	59R2W-60/64	60R2W-60/66	61R1W-10/14	66R4W-101/103
Depth (mbsf):	1603.10	1612.25	1613.70	1623.68	1633.42	1641.22	1695.05
Lithology:	Lapilli	Volcanic block	Volcanic block	Lapilli	Lapilli	Lapilli tuff	Volcanic block Tuff breccia and lapilli tuff
Host rock:	Lapilli stone	Tuff breccia	Tuff breccia	Lapilli tuff	Tuff breccia	-	
Pr	—	—	1.38	—	4.00	—	—
Nd	—	—	7.04	—	19.80	—	—
Sm	—	—	2.19	—	5.58	—	—
Eu	—	—	0.805	—	1.87	—	—
Gd	—	—	2.83	—	7.83	—	—
Tb	—	—	0.498	—	1.34	—	—
Dy	—	—	3.26	—	9.33	—	—
Ho	—	—	0.704	—	2.18	—	—
Er	—	—	2.10	—	6.85	—	—
Tm	—	—	0.298	—	0.993	—	—
Yb	—	—	2.03	—	6.49	—	—
Lu	—	—	0.309	—	1.02	—	—
Hf	—	—	1.50	—	2.23	—	—
Ta	—	—	0.044	—	0.079	—	—
Tl	—	—	0.005	—	0.079	—	—
Pb	—	—	1.51	—	1.69	—	—
Th	—	—	0.336	—	0.565	—	—
U	—	—	0.123	—	0.23	—	—
Unit:	Unit VII						
Sample ID:	66R5W-97/99	69R3W-9/11	70R2W-101/105	70R4W-129/131	70R6W-35/37	71R2W-13/15	71R2W-69/71
Depth (mbsf):	1696.52	1712.27	1721.42	1724.49	1726.50	1729.91	1730.47
Lithology:	Volcanic block	Volcanic block	Volcanic block	Lapilli	Lapilli	Volcanic block	Volcanic block
Host rock:	Tuff breccia	Tuff breccia	Volcanic breccia	Lapilli stone	Lapilli tuff	Not recovered	Not recovered
Major element (wt%) by XRF							
SiO ₂	56.87	53.32	55.91	52.94	51.34	56.49	52.44
TiO ₂	0.95	1.09	0.96	1.05	1.30	1.07	1.14
Al ₂ O ₃	16.79	18.99	18.99	21.14	19.62	18.20	19.67
Fe ₂ O ₃	9.35	9.32	8.39	7.35	10.04	8.26	9.31
MnO	0.22	0.20	0.20	0.16	0.21	0.22	0.17
MgO	3.93	4.62	3.42	3.39	4.77	2.85	4.00
CaO	5.69	6.81	7.25	9.09	8.16	7.47	9.03
Na ₂ O	5.47	5.15	4.23	4.34	4.25	4.42	3.68
K ₂ O	0.64	0.53	0.83	0.63	0.59	0.87	0.48
P ₂ O ₅	0.19	0.23	0.21	0.21	0.20	0.19	0.23
Total	100.10	100.25	100.40	100.29	100.46	100.03	100.14
LOI	2.49	2.64	2.30	1.51	2.55	1.68	2.33
Trace element (ppm) by XRF							
Ba	86.0	108.6	79.1	61.0	98.5	123	77.0
Ni	21.7	13.7	9.4	18.8	14.5	11	10.8

(Continues)

TABLE 1 (Continued)

Unit:	Unit VII						
Sample ID:	66R5W-97/99	69R3W-9/11	70R2W-101/105	70R4W-129/131	70R6W-35/37	71R2W-13/15	71R2W-69/71
Depth (mbsf):	1696.52	1712.27	1721.42	1724.49	1726.50	1729.91	1730.47
Lithology:	Volcanic block	Volcanic block	Volcanic block	Lapilli	Lapilli	Volcanic block	Volcanic block
Host rock:	Tuff breccia	Tuff breccia	Volcanic breccia	Lapilli stone	Lapilli tuff	Not recovered	Not recovered
Cu	33.3	40.0	32.3	53.5	41.9	25.8	38.4
Zn	92.8	96.3	95.2	88.3	118.8	98	89.8
Pb	2.9	3.2	1.9	3.3	1.7	1.6	3.0
Rb	8.2	5.8	8.5	6.8	6.6	8.8	5.0
Sr	220.6	262.5	276.1	296.9	280.1	257.1	338.4
Y	27.9	35.9	34.0	33.8	35.5	29.9	32.1
Zr	88.9	102.9	89.2	92.0	94.2	84.1	92.4
Nb	(1.4)	(1.5)	(0.9)	(1.1)	(1.2)	(1.1)	(1.0)
Cr	45.3	25.6	12.3	29.8	16.9	17.5	15.3
V	234.5	278.0	251.8	296.3	395.9	316.4	325.5

Trace element (ppm) by ICP-MS

Sc	—	26.8	—	23.8	32.5	—	28.3
Co	—	18.8	—	17.4	23.8	—	21.7
Ni	—	11.2	—	15.6	13.5	—	9.9
Cu	—	37.5	—	49.1	40.8	—	35.1
Rb	—	4.66	—	5.53	5.30	—	4.06
Sr	—	242	—	279	267	—	320
Y	—	34.2	—	32.0	34.9	—	30.7
Zr	—	102	—	89.8	96.0	—	92.7
Nb	—	1.20	—	1.15	1.29	—	1.24
Cs	—	0.14	—	0.15	0.10	—	0.30
Ba	—	116	—	76.2	108	—	73.8
La	—	5.92	—	4.71	4.19	—	6.17
Ce	—	17.8	—	13.5	13.3	—	16.3
Pr	—	2.80	—	2.27	2.26	—	2.52
Nd	—	14.1	—	11.6	11.5	—	12.6
Sm	—	4.20	—	3.65	3.71	—	3.79
Eu	—	1.340	—	1.260	1.260	—	1.250
Gd	—	5.18	—	4.60	4.70	—	4.64
Tb	—	0.898	—	0.814	0.850	—	0.799
Dy	—	5.86	—	5.46	5.77	—	5.28
Ho	—	1.270	—	1.180	1.260	—	1.130
Er	—	3.83	—	3.56	3.82	—	3.39
Tm	—	0.568	—	0.521	0.555	—	0.495
Yb	—	3.80	—	3.48	3.68	—	3.28
Lu	—	0.582	—	0.521	0.562	—	0.499
Hf	—	2.96	—	2.62	2.76	—	2.67
Ta	—	0.085	—	0.081	0.089	—	0.086
Tl	—	0.041	—	0.056	0.055	—	0.036
Pb	—	2.89	—	2.24	1.71	—	2.13

(Continues)

TABLE 1 (Continued)

Unit:	Unit VII						
Sample ID:	66R5W-97/99	69R3W-9/11	70R2W-101/105	70R4W-129/131	70R6W-35/37	71R2W-13/15	71R2W-69/71
Depth (mbsf):	1696.52	1712.27	1721.42	1724.49	1726.50	1729.91	1730.47
Lithology:	Volcanic block	Volcanic block	Volcanic block	Lapilli	Lapilli	Volcanic block	Volcanic block
Host rock:	Tuff breccia	Tuff breccia	Volcanic breccia	Lapilli stone	Lapilli tuff	Not recovered	Not recovered
Th	—	0.753	—	0.652	0.692	—	0.669
U	—	0.344	—	0.312	0.280	—	0.345
Unit:	Unit VII					Igneous Unit 1	
Sample ID:	72R2W-109/112	75R3W-70/72	78R1W-129/131	79R1W-46/48	79R2W-38/40	35R1W-123/125	35R2W-44/46
Depth (mbsf):	1740.62	1770.72	1793.60	1797.27	1798.58	1389.34	1389.97
Lithology:	Volcanic block	Volcanic block	Lapilli	Lapilli	Volcanic block	Sheet Lapilli tuff, lapilli stone	Sheet Lapilli tuff, lapilli stone
Host rock:	Tuff breccia	Lapilli tuff	Not recovered	Lapilli stone	Lapilli stone	stone	stone

Major element (wt%) by XRF

SiO ₂	53.18	56.61	56.18	53.87	53.92	77.32	74.00
TiO ₂	0.81	0.78	0.80	1.14	1.12	0.29	0.29
Al ₂ O ₃	18.68	16.73	17.73	21.18	21.16	11.99	13.81
Fe ₂ O ₃	8.27	6.19	6.65	6.28	6.30	2.14	1.99
MnO	0.21	0.19	0.14	0.10	0.08	0.03	0.05
MgO	5.88	4.68	5.11	3.67	3.80	0.22	0.22
CaO	10.59	10.53	8.61	7.78	7.92	0.60	1.24
Na ₂ O	2.76	2.73	3.07	5.01	5.25	6.64	7.55
K ₂ O	0.17	0.22	0.45	0.89	0.35	0.32	0.55
P ₂ O ₅	0.27	0.98	0.54	0.26	0.22	0.10	0.08
Total	100.83	99.63	99.27	100.17	100.11	99.66	99.77
LOI	2.33	1.82	3.07	2.05	2.11	2.27	2.53

Trace element (ppm) by XRF

Ba	29.3	Nd	52.6	288.4	90.0	n.d.	n.d.
Ni	51.1	54.6	50.7	24.3	20.9	n.d.	n.d.
Cu	57.9	63	26	49	20.7	2.8	2.0
Zn	83.1	102	98	80	62.5	29.7	27.6
Pb	1.5	2.2	1.4	2.5	3.2	3.3	1.3
Rb	3.7	4.6	8.5	6.9	3.6	2.8	4.1
Sr	230.7	267.9	265	308.3	286.2	n.d.	n.d.
Y	25.3	22.3	34.9	28.2	23.8	19.6	16.7
Zr	44.8	42.2	48.5	98	96.8	104.9	106.7
Nb	(0.6)	(0.8)	(0.8)	(1.7)	(1.5)	(0.9)	(0.9)
Cr	195.9	336.2	193.8	25.3	23.3	4.9	3.3
V	322.4	301.2	359	247.8	254.5	35.4	40.3

Trace element (ppm) by ICP-MS

Sc	—	—	—	26.0	—	3.85	—
Co	—	—	—	16.1	—	1.78	—
Ni	—	—	—	21.4	—	1.11	—
Cu	—	—	—	44.1	—	3.15	—
Rb	—	—	—	5.94	—	1.49	—

(Continues)

TABLE 1 (Continued)

Unit:	Unit VII					Igneous Unit 1	
	72R2W-109/112	75R3W-70/72	78R1W-129/131	79R1W-46/48	79R2W-38/40	35R1W-123/125	35R2W-44/46
Sample ID:							
Depth (mbsf):	1740.62	1770.72	1793.60	1797.27	1798.58	1389.34	1389.97
Lithology:	Volcanic block	Volcanic block	Lapilli	Lapilli	Volcanic block	Sheet Lapilli tuff, lapilli stone	Sheet Lapilli tuff, lapilli stone
Host rock:	Tuff breccia	Lapilli tuff	Not recovered	Lapilli stone	Lapilli stone		
Sr	—	—	—	293	—	6.47	—
Y	—	—	—	26.6	—	16.2	—
Zr	—	—	—	96.8	—	93.6	—
Nb	—	—	—	1.47	—	0.80	—
Cs	—	—	—	0.11	—	0.02	—
Ba	—	—	—	297	—	11.7	—
La	—	—	—	5.46	—	6.03	—
Ce	—	—	—	14.8	—	14.2	—
Pr	—	—	—	2.29	—	1.88	—
Nd	—	—	—	11.6	—	8.05	—
Sm	—	—	—	3.30	—	1.90	—
Eu	—	—	—	1.190	—	0.569	—
Gd	—	—	—	3.90	—	2.06	—
Tb	—	—	—	0.648	—	0.356	—
Dy	—	—	—	4.30	—	2.18	—
Ho	—	—	—	0.968	—	0.553	—
Er	—	—	—	3.16	—	1.82	—
Tm	—	—	—	0.489	—	0.304	—
Yb	—	—	—	3.39	—	2.11	—
Lu	—	—	—	0.525	—	0.349	—
Hf	—	—	—	2.72	—	2.61	—
Ta	—	—	—	0.105	—	0.075	—
Tl	—	—	—	0.058	—	0.014	—
Pb	—	—	—	2.31	—	2.79	—
Th	—	—	—	0.815	—	0.988	—
U	—	—	—	0.384	—	0.419	—

Note: Data in bold are applied the alkali fusion.

Abbreviations: —, not analyzed; ICP-MS, inductively coupled plasma-mass spectrometry; LOI, loss on ignition; n.d., not detected; XRF, X-ray fluorescence.

How much transport affected the rest of Unit VII is more ambiguous. Some intervals are clearly graded, stratified, and/or polymictic, attesting to lateral transport and accidental pick-up from the substrate. The provenance of other intervals cannot be assessed with confidence because of poor core recovery. Nevertheless, apart from a few fine-grained intervals, most of Unit VII is made of thick beds of angular, coarse ash-size to lapilli-size hyaloclasts and lava clasts, strongly suggesting that they are derived from sources less than a few hundred meters away, thus not associated with long-distance transport. Most of the analyzed clasts are atypically large (2–42 cm) and dense (non- to moderately vesicular). The provenance of these coarse clasts may be linked to accidental pick-up from the substrate during local avalanching of the hyaloclastites, or they may

represent in situ subsurface intrusive hyaloclasts. The large range in textures shown in these clasts therefore makes them representative of a broader region upslope (hundreds of meters to a few kilometers), and not only derived from a single locality or vent. Large chemical variations of clasts from Unit VII are consistent with this provenance model.

2.2 | Samples and methods

Samples were selected from Unit IV to Unit VII of Site U1437 (Figure 2; Table 1). The cores are overall green in color, suggesting low-grade burial metamorphism (Tamura et al., 2015b). Samples from Unit VII

were collected between 1461 and 1799 mbsf. Two samples (42R4W-106/112 and 61R1W-10/14) are lapilli tuff in grain size, following the onboard classification (Tamura et al., 2015a). The other 23 samples are made of individual volcanic clasts (lapilli to block in size); the single dense clasts are part of clast-supported or matrix-supported, polymictic (lava and fiamme) breccia. Most clasts have phenocrysts of pyroxene and/or feldspar; three (58R1W-34/36, 58R2W-36/38, and 69R3W-9/11) have additional amphibole as phenocrysts. Samples from Unit VI were collected between 1391 and 1453 mbsf. One (41R4W-129/133) is lapilli tuff in grain size (Tamura et al., 2015a), and others are individual volcanic clasts (lapilli in size). Igneous Unit 1 is a peperitic rhyolite

intrusion, and samples were collected for analyses from 1389.34 and 1389.97 mbsf. Samples from Unit V were collected between 1215 and 1294 mbsf. One (17R2W-125/127) is a lapilli stone in grain size, and other three are lapilli tuff (Tamura et al., 2015a). Sample from Unit IV is a lapilli tuff collected from 1119.9 mbsf.

2.3 | Sample preparation

Rocks were sawn and polished to extract individual clasts. These clasts were crushed into pebble sizes (5–10 mm) and soaked in plenty

JB-2 (ppm)	This study (XRF, $n = 2$)	This study (ICP-MS, $n = 2$)	Imai et al. (1995)	Chang et al. (2003)
Zn	114.3	—	108	—
Cr	24.2	—	28.1	—
V	589.7	—	575	—
Sc	—	51.2	53.5	—
Co	—	36.7	38	—
Ni	12.8	14.0	16.6	—
Cu	225.6	220.3	225	—
Rb	7.4	6.11	7.37	6.91
Sr	174.6	169	178	182.6
Y	21.2	21.5	24.9	23.3
Zr	43.5	45.8	51.2	49.8
Nb	0.5	0.46	1.58	0.510
Cs	—	0.77	0.85	—
Ba	206.9	213.0	222	215.5
La	—	2.15	2.35	2.14
Ce	—	6.28	6.76	6.37
Pr	—	1.10	1.01	1.09
Nd	—	6.1	6.63	6.13
Sm	—	2.16	2.31	2.21
Eu	—	0.784	0.86	0.803
Gd	—	3.09	3.28	3.06
Tb	—	0.562	0.6	0.557
Dy	—	3.83	3.73	3.83
Ho	—	0.835	0.75	0.832
Er	—	2.51	2.6	2.53
Tm	—	0.364	0.41	0.368
Yb	—	2.43	2.62	2.49
Lu	—	0.371	0.4	0.376
Hf	—	1.48	1.49	1.50
Ta	—	0.029	0.13	0.043
Tl	—	0.031	0.042	—
Pb	4.65	4.98	5.36	5.48
Th	—	0.249	0.35	0.282
U	—	0.150	0.18	0.163

TABLE 2 Result for standard rock (JB-2) compositions

Abbreviations: —, no data; ICP-MS, inductively coupled plasma-mass spectrometry.

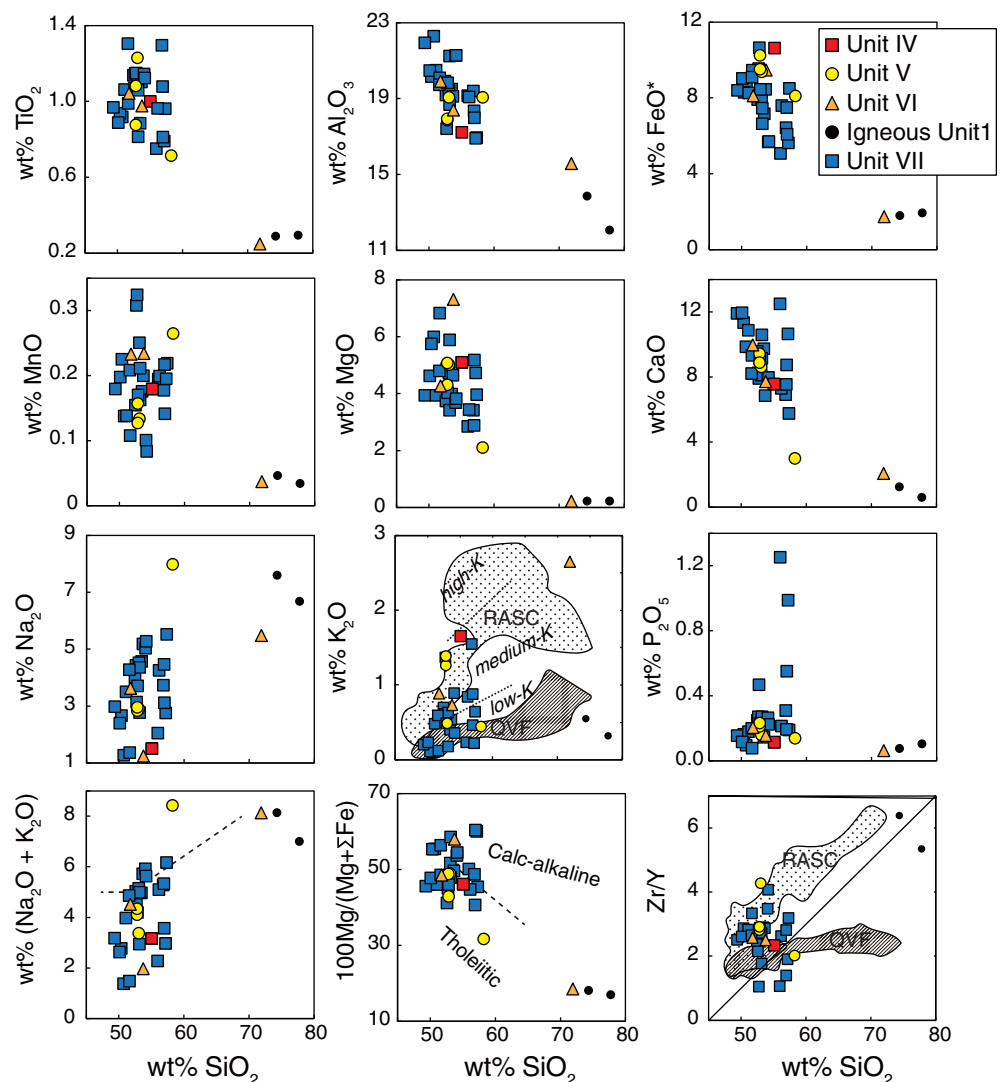
of slowly flooded hot water of $\sim 40^\circ\text{C}$ for 2 weeks. Then, these clasts were put into a glass beaker with distilled water, which was boiled in a microwave oven. The addition of fresh distilled water and boiling were repeated until an addition of silver nitrate solution stops to precipitate silver chloride. After the desalinization, all samples were washed with pure water and acetone using an ultrasonic cleaner. Coarse samples were pounded in an iron mortar, and altered pieces were removed by hand picking as much as possible. All samples were pulverized using a polycarbonate tube and alumina rod.

2.4 | Major and trace element analyses

For analysis of major elements, a mixture of 0.4 g of sample powder and 4 g of $\text{Li}_2\text{B}_4\text{O}_7$ was fused and vitrified. This glass bead was analyzed using a Rigaku Simultix 12, X-ray fluorescence (XRF) analyzer, following the method of Tani, Kawabata, Chang, Sato, and Tatsumi (2006). Accuracy and reproducibility for major elements are better than 1% and better than 2% relative standard deviation (2 standard deviation), respectively.

The concentrations of Ba, Ni, Cu, Zn, Pb, Rb, Sr, Y, Zr, Nb, Cr, and V were measured using pressed powder pellets and a Rigaku RIX3000 (XRF), following the method of Goto and Tatsumi (1996). For selected seven samples from Unit VII, Unit V, and Igneous Unit 1, the concentrations of 31 trace elements (including rare earth element [REE]) were determined by inductively coupled plasma-mass spectrometry (ICP-MS) using an Agilent 7500ce (Agilent Technologies, Santa Clara, California). Rock powders were digested in a HClO_4/HF mixture. After reaching dryness, the samples were dissolved in 2% HNO_3 with trace HF. Indium and bismuth were added as internal standards (Chang, Shibata, Shinotsuka, Yoshikawa, & Tatsumi, 2003). Oxide and hydroxide interferences were subtracted from the peaks of Eu and Gd. The concentrations of Y, Zr, Ho, Er, Tm, Yb, Lu, Hf, and Th from the sample of Igneous Unit 1 were measured using alkali fusion for decomposition because of the presence of zircon (Senda, Kimura, & Chang, 2014). The analytical results of well-established reference standard (JB-2) agreed very well with recommended values by Imai, Terashima, Itoh, and Ando (1995) and Chang et al. (2003), demonstrating that trace element determinations had high accuracy. Results for standard

FIGURE 3 SiO_2 variation diagrams of wt% SiO_2 vs major element oxides (wt%), total alkali, Mg number values ($100 \text{Mg}/[\text{Mg} + \Sigma\text{Fe}]$), and Zr/Y ratio, for samples from Units IV to VII and Igneous Unit 1. The fields in SiO_2 vs K_2O and SiO_2 vs Zr/Y plot show published data; QVF, Izu Quaternary volcanic front data from Hochstaedter et al. (2000, 2001), Shukuno et al. (2006), Tamura et al. (2005, 2007, 2009), R. N. Taylor and Nesbitt (1998), and Tollstrup et al. (2010); RASC, rear-arc seamount chains from Hochstaedter et al. (2000, 2001), Ishizuka, Uto, and Yuasa (2003), Ishizuka, Uto, Yuasa, and Hochstaedter (2002), Machida and Ishii (2003), Machida, Ishii, Kimura, Awaji, and Kato (2008), and Tollstrup et al. (2010). The dashed lines in SiO_2 vs K_2O plot show the boundary between low-K, medium-K, and high-K (Gill, 1981). Calc-alkaline and tholeiitic boundaries in SiO_2 vs Mg-number plot are after Miyashiro (1974). All but three with rhyolitic composition show a broad trend, with a narrow SiO_2 (49–58 wt%), mostly ranging from basalts to andesites but having three basaltic trachyandesites and two trachyandesites in the SiO_2 - $\text{Na}_2\text{O} + \text{K}_2\text{O}$ plot after Le Maitre (2002) shown by the dashed line



rock sample (JB-2) are presented in Table 2. We focus mainly on Units VII and V, in the following chapters.

3 | RESULTS

Major and trace element concentrations in the samples from Unit IV to Unit VII (Figure 2) are presented in Table 1 and shown in Figures 3–6. Several samples of Unit VII had anomalously high MnO and/or P₂O₅, indicating the possibility of secondary alteration; therefore, in the following discussion of major elements, we excluded the samples with more than 0.3 wt% of MnO and/or 0.4 wt% of P₂O₅ (43R2W-98/101, 59R2W-60/64, 60R2W-60/66, 75R3W-70/72, and 78R1W-129/131). Major elements in the following discussion have been normalized to 100 % on a volatile-free basis with total iron calculated as FeO.

Variation diagrams of wt% SiO₂ vs major element oxides (wt%), total alkali, Mg values (100 Mg/[Mg + ΣFe]), and Zr/Y ratio are shown in Figure 3. All but three with rhyolitic composition show a broad trend, with a narrow SiO₂ (49–58 wt%), mostly ranging from basalts to andesites but having three basaltic trachyandesites and two trachyandesites in the SiO₂ vs (Na₂O + K₂O) plot after Le Maitre (2002) (Figure 3). These samples also plot in low- to medium-K fields in the SiO₂ vs K₂O plot of Gill (1981) (Figure 3). Many of Unit VII samples are low-K basalts and andesites, which are different from medium-K rocks of rear-arc seamount chains. Mg numbers of basalts and andesites range from 31 to 59, and they are plotted both in the calc-alkaline and tholeiitic fields of Miyashiro (1974) (Figure 3). Four samples from Unit V are plotted in the tholeiitic field, but samples from Unit VII range from tholeiitic to calc-alkaline fields, which variation is often observed in the respective arc volcanoes. Many samples from Unit VII have higher Al₂O₃ and lower FeO* than four samples of Unit V, and these characteristics are similar to volcanoes of the Oligocene volcanic front (Tamura et al., 2010).

Two samples from Unit V have high K₂O contents (1.26 and 1.38 wt%) and have LREE-enriched patterns similar to those of the rear-arc seamount chain basalts (Figure 4a). REE patterns of selected eight samples from Unit VII are flat or concave with a maximum at Nd, and are neither similar to the LREE-enriched rear-arc

seamount chains, nor to the LREE-depleted Quaternary volcanic front basalts (Figure 4b). Kinan Escarpment basalts, which had erupted at the Shikoku Basin, southwest of the Izu arc (Figure 1a), have distinctive Ce anomalies (Figure 4b), which are also different from that of Unit VII. Recent extensional zone basalts have relatively gently sloped patterns but are more enriched in LREE compared to heavy rare earth element (HREE) and are different from those of Unit VII (Figure 4b).

Figure 5 shows N-mid-ocean ridge basalt normalized incompatible element patterns for Unit V, Igneous Unit 1, and Unit VII. The differences between Unit V and Unit VII are clearly shown in these trace element patterns. HREE contents of Unit V overlap those of Unit VII, but Nb and Ta contents are much more depleted in Unit VII than in Unit V. Such strong and weak depletions of Nb and Ta were observed in Pagan volcano of Mariana volcanic front and northwest Rota-1 volcano

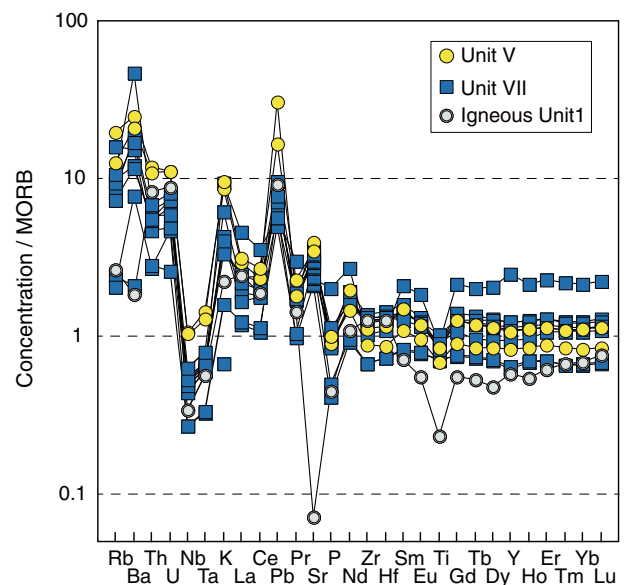


FIGURE 5 Normal (N)-MORB normalized incompatible element patterns for Unit V, Unit VII, and Igneous Unit 1. N-MORB composition is from Sun and McDonough (1989). The depletions in Nb and Ta of Unit VII are much larger than those of Unit V

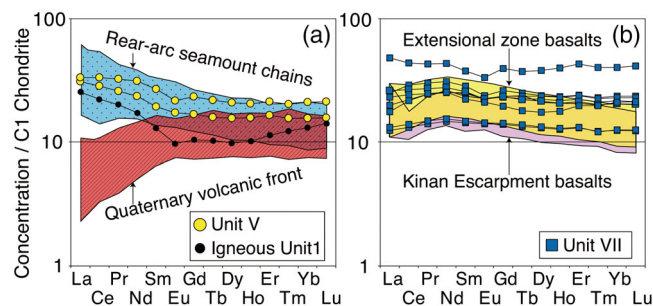


FIGURE 4 C1 chondrite-normalized (McDonough & Sun, 1995) rare earth element (REE) patterns. (a) REE patterns of Unit V and Igneous Unit 1. The fields for Quaternary volcanic front (< 55 wt% SiO₂) and rear-arc seamount chains (< 55 wt% SiO₂) are from the sources as for Figure 3. (b) REE patterns of Unit VII samples. The fields of extensional zone basalts from Tollstrup et al. (2010) and Kinan Escarpment basalts from Ishizuka et al. (2009) have relatively concave REE patterns with a maximum at Nd and negative Ce anomalies, respectively; neither are similar to the Unit VII

of Mariana rear-arc, respectively (Tamura et al., 2014). Thus, in terms of the negative anomalies of Nb and Ta, Unit VII and Unit V are similar to the volcanic front and the rear-arc, respectively. Interestingly, Igneous

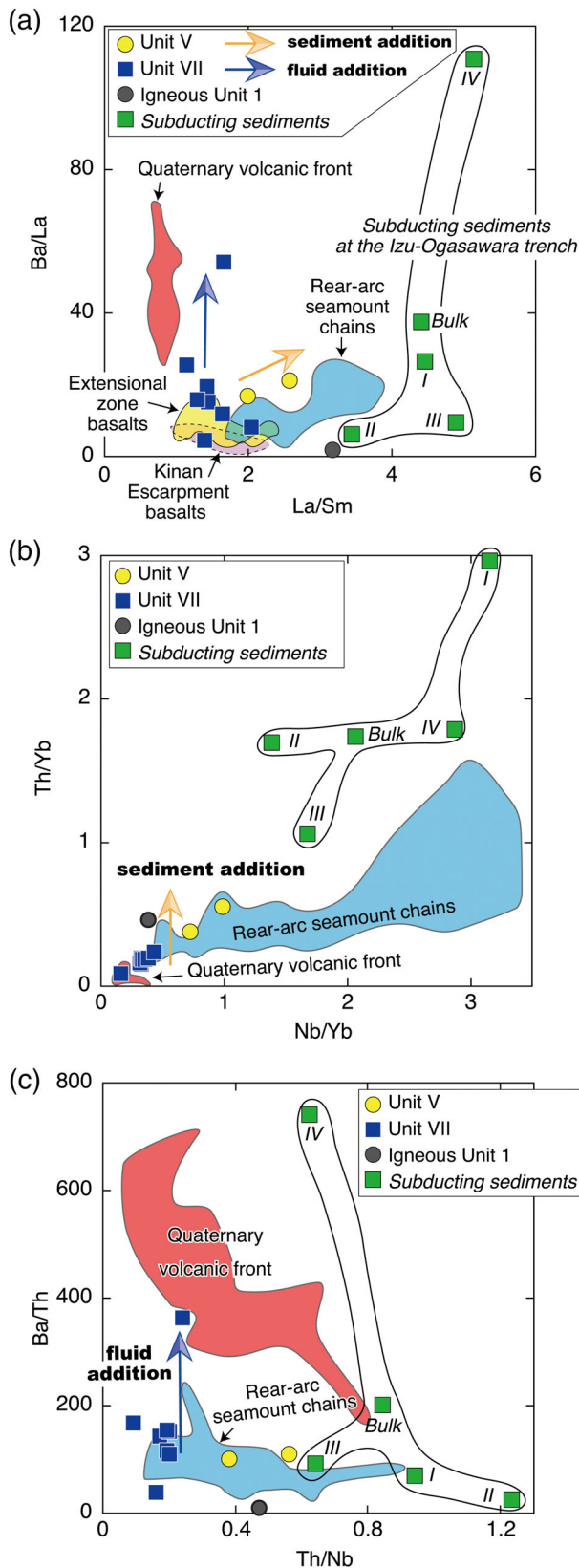


FIGURE 6 Legend on next column.

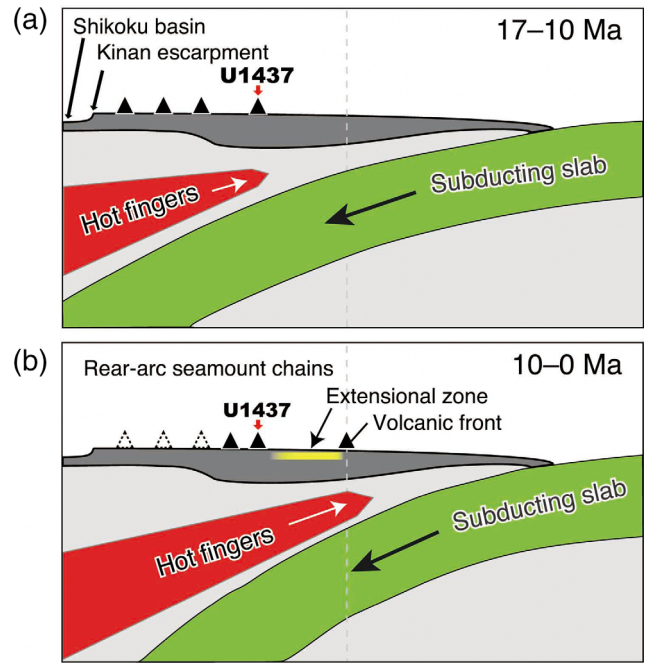


FIGURE 7 Schematic diagrams showing the evolution of the Izu arc system from (a) 17–10 Ma to (b) 10–0 Ma. Eastward intrusions of hot fingers into the Izu-Ogasawara arc mantle wedge at about 17 Ma had restarted arc volcanism after vigorous volcanism accompanied the opening of the Shikoku and Parece Vera Basins. (a) The subducting slab might have been shallower just after the cessation of the Shikoku Basin opening. (b) Hot fingers intruded into the mantle wedge and the slab steepened with time, resulting in a trench-ward migration of the volcanic front, extensional zone volcanism, and the rear-arc seamount chain type volcanism

Unit 1 is rhyolitic in composition, and its incompatible elements are generally lower than in basalts and basaltic andesites of Units V and VII. Igneous Unit 1 is highly depleted in Sr and Ti in particular (Figure 5).

4 | DISCUSSION

4.1 | Volcanic front vs rear-arc

The geochemical differences between volcanic front and rear-arc volcanoes could be related to spatial variations in subduction components within the subducting plate, which were added at different depths in the overlying mantle wedge during subduction before or during its melting (Ishizuka et al., 2006; Ishizuka, Taylor, Milton, & Nesbitt, 2003; Tamura et al., 2007; Tamura et al., 2014). The mantle

FIGURE 6 (a) Variation of Ba/La vs La/Sm for Site U1437 samples. Ba/La and La/Sm are proxies for additions of fluid and sediment-melt components derived from the subducting slab, respectively. (b) Variation of Th/Yb vs Nb/Yb. Th/Yb is a proxy for sediment addition. (c) Variation of Ba/Th vs Th/Nb. Ba/Th is a proxy for fluid addition. Published data are same as for Figure 4. Subducting sediments at the Izu-Ogasawara trench are from Plank, Kelley, Murray, and Stern (2007)

wedge might also have variations resulting from hot and low-velocity mantle materials (hot fingers; Tamura et al., 2002) intruding into the mantle wedge. In this scenario, the magma is first extracted beneath the rear-arc and then extracted again as the depleted mantle moves toward the volcanic front where it is fluxed by fluids from the slab (Hochstaedter et al., 2000; Hochstaedter et al., 2001). The geochemical signature of the generated magmas reflects the subduction components and the original mantle wedge (Hochstaedter et al., 2001; Straub, Woodhead, & Arculus, 2015; Tollstrup et al., 2010). Tamura et al. (2014) found that these distinct subduction components generate two primary magmas at the single volcanic front volcano of Pagan, Mariana arc, and suggested that these two subduction components can exist separately, because the hydrous fluid is a hydrous carbonate, which is immiscible with a silicate melt (sediment melt) (Tamura et al., 2014).

In summary, the volcanic front and rear-arc magmas are generated through partial melting of the underlying mantle wedge that contains different subduction components from the subducting slab. The dominant subduction component beneath the volcanic front is a hydrous fluid, whereas it is a sediment melt beneath rear-arc volcanoes. However, as mentioned above, a sediment melt could also coexist with a hydrous fluid beneath the volcanic front. In that case, the subduction component at the volcanic front could be characterized by diverse proportions of silicate melts and hydrous fluids derived from the subducting plate, whereas the hydrous fluids are seldom in the rear-arc.

Diagrams a, b, and c in Figure 6 show Ba/La vs La/Sm, Th/Yb vs Nb/Yb, and Ba/Th vs Th/Nb of selected Unit V and Unit VII samples. Ba/La and Ba/Th, and La/Sm and Th/Yb are proxies of subduction components that could represent H₂O-dominant fluids and sediment melts, respectively (Hochstaedter et al., 2001; Pearce, 2008). Samples from the Quaternary volcanic front (< 55 wt% SiO₂) have high Ba/La and Ba/Th ratios, suggesting that their subduction components are fluid dominated. Lavas from the rear-arc seamount chains (< 55 wt% SiO₂) have relatively higher La/Sm and Th/Yb and lower Ba/La ratios, suggesting subduction components that are dominated by sediment melts. REE patterns of the volcanic front and the rear-arc are consistent with this (Figure 4a); the LREE-enriched patterns of the rear-arc partly reflect sediment melts that can transport REE. Unit V samples show a rear-arc affinity, but Unit VII samples show a wide range of Ba/La and Ba/Th and La/Sm are higher than Quaternary volcanic front. La/Sm values of Unit VII are similar to values of Oligocene volcanic front (Tamura et al., 2010), and the strong depletion of Nb and Ta compared to heavy REE in Unit VII are also similar to the volcanic front (Tamura et al., 2010).

4.2 | Geochemical comparison with other volcanic areas near Site U1437

Samples from Site U1437 are compared to volcanic rocks from the middle part of the Izu arc in Figures 4 and 6. Selected Unit V lapilli tuff have REE patterns and subduction components that are similar to the rear-arc seamount chains (Figures 4a and 6), and the ~8 Ma

stratigraphic age of these samples (Figure 2) corresponds to the radiometric age of nearby rear-arc seamount chain volcanoes (Ishizuka, Uto, & Yuasa, 2003). This indicates that these Unit V samples have been reworked from neighboring rear-arc seamounts at ~8 Ma.

Unit VII samples have flat patterns or concave REE patterns with a maximum at Nd (Figure 4b). Some of the extensional zone basalts (Tollstrup et al., 2010) between the volcanic front and the rear-arc seamount chains have concave REE patterns with a maximum at Nd (Figure 4c). Their low Ba/La and La/Sm ratios also are similar to some of Unit VII (Figure 6). Extensional zone basalts are related to rifting within the Izu arc. They have been influenced by subduction components depending on the distance from the volcanic front (Hochstaedter et al., 2001).

The Kinan Escarpment is the boundary between the central part (19–15 Ma) and the eastern part (23–19 Ma) of the Shikoku Basin recognized by magmatic anomalies (Okino, Shimakawa, & Nagaoka, 1994). Kasuga and Ohara (1997) propose that this escarpment is a large normal fault that formed soon after the back-arc spreading ceased (15.69–11.8 Ma; Ishizuka, Yuasa, Taylor, & Sakamoto, 2009). Kinan Escarpment basalts (Ishizuka et al., 2009) have negative Ce anomalies (Figure 4d), which are different from Units V and VII. In the eastern part of the Shikoku Basin, there is additional post-spreading volcanism, that is, the East Shikoku Basin seamounts (14.39–11.04 Ma; Ishizuka et al., 2009). Ishizuka et al. (2009) show that these seamounts have a slab signature similar to that of the rear-arc seamount chains.

The wide variations in Ba/La and Ba/Th in Unit VII lavas (Figure 6) suggest the transient nature of fluid addition from the subducting plate, which might represent a prologue to a renaissance of active arc volcanism in the Izu-Ogasawara arc.

4.3 | The early Izu rear-arc magmatism

The rear-arc seamount chain-type volcanism occurred at about 17–8 Ma in the western part of this broader zone (i.e. East Shikoku Basin seamounts and the westernmost seamounts of the chains), and migrated to the eastern part of the chains over time during 8–3 Ma (Ishizuka et al., 1998; Ishizuka et al., 2009; Ishizuka, Uto, & Yuasa, 2003). Ishizuka et al. (2009) propose that this migration was caused by steepening of the subducting slab. At Site U1437, volcanic front and/or rift-type magmatism (Unit VII) is overlain by sediments from the rear-arc seamount chain-type magmatism (Unit V). The difference between Units VII and V indicates a temporal change of the subduction components, and supports the slab steepening hypothesis. Moreover, intrusions of hot fingers into the mantle wedge could play an important role in the genesis of arc volcanoes (Tamura, 2003; Tamura et al., 2002). It may be possible that eastward intrusions of hot fingers into the Izu-Ogasawara arc mantle wedge at about 17–15 Ma had restarted arc volcanism after the vigorous volcanism that accompanied the opening of the Shikoku and Parece Vera Basins. The subducting slab might have been shallower immediately after the cessation of the Shikoku

Basin opening (Figure 7a), and followed by intrusion of hot fingers into the mantle wedge. The slab steepened with time, resulting in a trench-ward migration of the volcanic front, accompanied by extensional zone volcanism and rear-arc seamount chain-type volcanism (Figure 7b).

5 | CONCLUSIONS

Drilling at Site U1437 in the IODP Expedition 350 has revealed temporal and spatial changes of magmatism in the Izu rear-arc. The geochemical characteristics of the hyaloclastites in Unit VII, the deepest part of the hole, represent the early arc magmatism (16–15 Ma) after the opening of the Shikoku Basin. These hyaloclastites reflect proximal submarine vents facies. Unit VII does not contain a rear-arc signature in terms of major element compositions and REE patterns. Instead, strong Nb and Ta depletions are similar to the composition of the volcanic front. The composition of Unit VII is similar to the Oligocene volcanic front in terms of major elements, and/or Pliocene to recent extensional zone basalts. The difference in rock composition between Units VII and V suggests intrusion of hot fingers in the mantle wedge and steepening of the subducting slab below Site U1437 after the formation of the Shikoku Basin.

ACKNOWLEDGEMENTS

We thank all R/V JOIDES Resolution crew, technical staff, and science party during IODP Expedition 350. Qing Chang of JAMSTEC is also thanked for his analytical guidance of trace elements by ICP-MS. This work was supported by JSPS KAKENHI Grant Numbers JP17H02987, JP16H06347, JP16H02742, and JP17K05686. M.J. acknowledges NERC grant NE/M005224/1, ECORD, and ANZIC for funding his research and travels. We much appreciate the comments and reviews of C. Timm and an anonymous reviewer and T. Kuritani (AE of *Island Arc*). Sources of geochemical data and map images used in Figures 1–6 are all listed in the figure captions.

ORCID

Tomoki Sato  <https://orcid.org/0000-0002-0076-0531>

Takashi Miyazaki  <https://orcid.org/0000-0002-0889-3961>

Yoshihiko Tamura  <https://orcid.org/0000-0002-3705-7815>

James B. Gill  <https://orcid.org/0000-0003-2584-9687>

Martin Jutzeler  <https://orcid.org/0000-0002-3720-6315>

REFERENCES

- Bandy, W. L., & Hilde, T. W. C. (1983). Structural features of the Bonin arc: Implications for its tectonic history. *Tectonophysics*, *99*, 331–353.
- Chang, Q., Shibata, T., Shinotsuka, K., Yoshikawa, M., & Tatsumi, Y. (2003). Precise determination of trace elements in geological standard rocks using inductively coupled plasma mass spectrometry (ICP-MS). *Frontier Research on Earth Evolution*, *1*, 357–362.
- Gill, J. B. (1981). *Orogenic andesites and plate tectonics*. Berlin, Germany: Springer.
- Gill, J. B., Bongiolo, E. M., Miyazaki, T., Hamelin, C., Jutzeler, M., DeBari, S., ... Yakavonis, M. (2018). Tuffaceous mud is a volumetrically important volcanoclastic facies of submarine arc volcanism and record of climate change. *Geochemistry, Geophysics, Geosystems*, *19*, 1217–1243. <https://doi.org/10.1002/2017GC007300>
- Goto, A., & Tatsumi, Y. (1996). Quantitative analysis of rock samples by an X-ray fluorescence spectrometer (II). *The Rigaku Journal*, *13*, 20–39.
- Hochstaedter, A., Gill, J., Peters, R., Broughton, P., Holden, P., & Taylor, B. (2001). Across-arc geochemical trends in the Izu-Bonin arc: Contributions from the subducting slab. *Geochemistry, Geophysics, Geosystems*, *2*, 2000GC000105. <https://doi.org/10.1029/2000GC000105>
- Hochstaedter, A., Gill, J. B., Taylor, B., Ishizuka, O., Yuasa, M., & Morita, S. (2000). Across-arc geochemical trends in the Izu-Bonin arc: Constraints on source composition and mantle melting. *Journal of Geophysical Research*, *105*, 495–512.
- Honda, S., Yoshida, T., & Aoike, K. (2007). Spatial and temporal evolution of arc volcanism in the northeast Honshu and Izu-Bonin Arcs: Evidence of small-scale convection under the island arc? *Island Arc*, *16*, 214–223.
- Imai, N., Terashima, S., Itoh, S., & Ando, A. (1995). 1994 compilation of analytical data for minor and trace elements in seventeen GSJ geochemical reference samples, "igneous rock series". *Geostandards Newsletter*, *19*, 135–213.
- Ishizuka, O., Taylor, R. N., Milton, J. A., & Nesbitt, R. W. (2003). Fluid-mantle interaction in an intra-oceanic arc: Constraints from high-precision Pb isotopes. *Earth and Planetary Science Letters*, *211*, 221–236. [https://doi.org/10.1016/S0012-821X\(03\)00201-2](https://doi.org/10.1016/S0012-821X(03)00201-2)
- Ishizuka, O., Taylor, R. N., Milton, J. A., Nesbitt, R. W., Yuasa, M., & Sakamoto, I. (2006). Variation in the mantle sources of the northern Izu arc with time and space — Constraints from high-precision Pb isotopes. *Journal of Volcanology and Geothermal Research*, *156*, 266–290. <https://doi.org/10.1016/j.jvolgeores.2006.03.005>
- Ishizuka, O., Uto, K., & Yuasa, M. (2003). Volcanic history of the back-arc region of the Izu-Bonin (Ogasawara) arc. *Geological Society, London, Special Publications*, *219*, 187–205.
- Ishizuka, O., Uto, K., Yuasa, M., & Hochstaedter, A. G. (1998). K-Ar ages from seamount chains in the back-arc region of the Izu-Ogasawara arc. *The Island Arc*, *7*, 408–421.
- Ishizuka, O., Uto, K., Yuasa, M., & Hochstaedter, A. G. (2002). Volcanism in the earliest stage of back-arc rifting in the Izu-Bonin arc revealed by laser-heating ⁴⁰Ar/³⁹Ar dating. *Journal of Volcanology and Geothermal Research*, *120*, 71–85.
- Ishizuka, O., Yuasa, M., Taylor, R. N., & Sakamoto, I. (2009). Two contrasting magmatic types coexist after the cessation of back-arc spreading. *Chemical Geology*, *266*, 274–296. <https://doi.org/10.1016/j.chemgeo.2009.06.014>
- Karig, D. E., & Moore, G. F. (1975). Tectonic complexities in the Bonin arc system. *Tectonophysics*, *27*, 97–118.
- Kasuga, S., & Ohara, Y. (1997). Evolution of the escarpments located in the Back-arc Basins in the Southern Waters of Japan-Mechanical boundary between sinking Back-arc Basins and Buoyant Active Island Arcs. *Report of Hydrographic Researches*, *33*, 39–51 (in Japanese with English abstract).
- Kodaira, S., Sato, T., Takahashi, N., Ito, A., Tamura, Y., Tatsumi, Y., & Kaneda, Y. (2007). Seismological evidence for variable growth of crust along the Izu intraoceanic arc. *Journal of Geophysical Research - Solid Earth*, *112*, B05104. <https://doi.org/10.1029/2006JB004593>
- Kodaira, S., Sato, T., Takahashi, N., Miura, S., Tamura, Y., Tatsumi, Y., & Kaneda, Y. (2007). New seismological constraints on growth of continental crust in the Izu-Bonin intra-oceanic arc. *Geology*, *35*, 1031–1034.
- Kodaira, S., Sato, T., Takahashi, N., Yamashita, M., No, T., & Kaneda, Y. (2008). Seismic imaging of a possible paleoarc in the Izu-Bonin intraoceanic arc and its implications for arc evolution processes. *Geochemistry, Geophysics, Geosystems*, *9*, Q10X01. <https://doi.org/10.1029/2008GC002073>
- Le Maitre, R. W. (2002). *A classification of igneous rocks and glossary of terms* (2nd ed.). Cambridge, England: Cambridge University Press.

- Machida, S., & Ishii, T. (2003). Backarc volcanism along the en echelon seamounts: The Enpo seamount chain in the northern Izu-Ogasawara arc. *Geochemistry, Geophysics, Geosystems*, 4(8), 9006. <https://doi.org/10.1029/2003GC000554>
- Machida, S., Ishii, T., Kimura, J.-I., Awaji, S., & Kato, Y. (2008). Petrology and geochemistry of cross-chains in the Izu-Bonin back arc: Three mantle components with contributions of hydrous liquids from a deeply subducted slab. *Geochemistry, Geophysics, Geosystems*, 9, Q05002. <https://doi.org/10.1029/2007GC001641>
- McDonough, W. F., & Sun, S. -S. (1995). The composition of the earth. *Chemical Geology*, 120, 223–253.
- Miyashiro, A. (1974). Volcanic rock series in island arcs and active continental margins. *American Journal of Science*, 274, 312–355.
- Okino, K., Ohara, Y., Kasuga, S., & Kato, Y. (1999). The Philippine Sea: New survey results reveal the structure and the history of the marginal basins. *Geophysical Research Letters*, 26, 2287–2290.
- Okino, K., Shimakawa, Y., & Nagaoka, S. (1994). Evolution of the Shikoku Basin. *Journal of Geomagnetism and Geoelectricity*, 46, 463–479.
- Pearce, J. A. (2008). Geochemical fingerprinting of oceanic basalts with applications to ophiolite classification and the search for Archean oceanic crust. *Lithos*, 100, 14–48.
- Plank, T., Kelley, K. A., Murray, R. W., & Stern, L. Q. (2007). Chemical composition of sediments subducting at the Izu-Bonin trench. *Geochemistry, Geophysics, Geosystems*, 8, 1–16. <https://doi.org/10.1029/2006GC001444>
- Schmitt, A. K., Konrad, K., Andrews, G. D. M., Horie, K., Brown, S. R., Koppers, A. A. P., ... Tamura, Y. (2018). $^{40}\text{Ar}/^{39}\text{Ar}$ ages and zircon petrochronology for the rear arc of the Izu-Bonin-Marianas intra-oceanic subduction zone. *International Geology Review*, 60, 956–976. <https://doi.org/10.1080/00206814.2017.1363675>
- Senda, R., Kimura, J.-I., & Chang, Q. (2014). Evaluation of a rapid, effective sample digestion method for trace element analysis of granitoid samples containing acid-resistant minerals: Alkali fusion after acid digestion. *Geochemical Journal*, 48, 99–103. <https://doi.org/10.2343/geochemj.2.0280>
- Shukuno, H., Tamura, Y., Tani, K., Chang, Q., Suzuki, T., & Fiske, R. S. (2006). Origin of silicic magmas and the compositional gap at Sumisu submarine caldera, Izu-Bonin arc, Japan. *Journal of Volcanology and Geothermal Research*, 156, 187–216.
- Straub, S. M., Woodhead, J. D., & Arculus, R. J. (2015). Temporal evolution of the Mariana Arc: Mantle wedge and subducted slab controls revealed with a tephra perspective. *Journal of Petrology*, 56, 409–439. <https://doi.org/10.1093/ptrology/egv005>
- Sun, S. -S., & McDonough, W. F. (1989). Chemical and isotopic systematics of oceanic basalts: Implications for mantle composition and processes. *Geological Society, London, Special Publications*, 42, 313–345.
- Suyehiro, K., Takahashi, N., Ariei, Y., & Yokoi, Y. (1996). Continental crust, crustal underplating, and low-Q upper mantle beneath an oceanic island arc. *Science*, 272, 390–392.
- Tamura, Y. (2003). Some geochemical constraints on hot fingers in the mantle wedge: Evidence from NE Japan. In R. D. Larter & P. T. Leat (Eds.), *Intra-oceanic subduction systems: Tectonic and magmatic processes* (Vol. 219, pp. 221–237). London: Geological Society.
- Tamura, Y., Busby, C. J., Blum, P., Guérin, G., Andrews, G. D. M., Barker, A. K., ... Yang, Y. (2015a). Expedition 350 methods. In Y. Tamura, C. J. Busby, P. Blume, & Expedition 350 Scientists (Eds.), *Proceedings of International Ocean Discovery Program, Expedition 350: Izu-Bonin-Mariana Rear Arc*. College Station, TX: International Ocean Discovery Program. <https://doi.org/10.14379/iodp.proc.350.102.2015>
- Tamura, Y., Busby, C. J., Blum, P., Guérin, G., Andrews, G. D. M., Barker, A. K., ... Yang, Y. (2015b). Site U1437. In Y. Tamura, C. J. Busby, P. Blume, & Expedition 350 Scientists (Eds.), *Proceedings of International Ocean Discovery Program, Expedition 350: Izu-Bonin-Mariana Rear Arc*. College Station, TX: International Ocean Discovery Program. <https://doi.org/10.14379/iodp.proc.350.104.2015>
- Tamura, Y., Gill, J. B., Tollstrup, D., Kawabata, H., Shukuno, H., Chang, Q., ... Tatsumi, Y. (2009). Silicic magmas in the Izu-Bonin oceanic arc and implications for crustal evolution. *Journal of Petrology*, 50, 685–723. <https://doi.org/10.1093/ptrology/egp017>
- Tamura, Y., Ishizuka, O., Aoike, K., Kawate, S., Kawabata, H., Chang, Q., ... Fiske, R. S. (2010). Missing Oligocene crust of the Izu-Bonin arc: Consumed or rejuvenated during collision? *Journal of Petrology*, 51, 823–846.
- Tamura, Y., Ishizuka, O., Sato, T., & Nichols, A. R. L. (2019). Nishinoshima volcano in the Ogasawara Arc: New continent from the ocean? *Island Arc*, 28, e12285. <https://doi.org/10.1111/iar.12285>
- Tamura, Y., Ishizuka, O., Stern, R. J., Nichols, A. R. L., Kawabata, H., Hirahara, Y., ... Embley, R. W. (2014). Mission immiscible: Distinct subduction components generate two primary magmas at Pagan volcano, Mariana Arc. *Journal of Petrology*, 55, 63–101. <https://doi.org/10.1093/ptrology/egt061>
- Tamura, Y., Sato, T., Fujiwara, T., Kodaira, S., & Nichols, A. (2016). Advent of continents: A new hypothesis. *Scientific Reports*, 6, 33517. <https://doi.org/10.1038/srep33517>
- Tamura, Y., Tani, K., Chang, Q., Shukuno, H., Kawabata, H., Ishizuka, O., & Fiske, R. S. (2007). Wet and dry basalt magma evolution at Torishima Volcano, Izu-Bonin Arc, Japan: The possible role of phengite in the downgoing slab. *Journal of Petrology*, 48, 1999–2031. <https://doi.org/10.1093/ptrology/egm048>
- Tamura, Y., Tani, K., Ishizuka, O., Chang, Q., Shukuno, H., & Fiske, R. S. (2005). Are arc basalts dry, wet, or both? Evidence from the Sumisu caldera volcano, Izu-Bonin arc, Japan. *Journal of Petrology*, 46, 1769–1803. <https://doi.org/10.1093/ptrology/egi033>
- Tamura, Y., & Tatsumi, Y. (2002). Remelting of an andesitic crust as a possible origin for rhyolitic magma in oceanic arcs: An example from the Izu-Bonin arc. *Journal of Petrology*, 43, 1029–1047.
- Tamura, Y., Tatsumi, Y., Zhao, D., Kido, Y., & Shukuno, H. (2002). Hot fingers in the mantle wedge: New insights into magma genesis in subduction zones. *Earth and Planetary Science Letters*, 197, 105–116.
- Tani, K., Kawabata, H., Chang, Q., Sato, K., & Tatsumi, Y. (2006). Quantitative analyses of silicate rock major and trace elements by X-ray fluorescence spectrometer: Evaluation of analytical precision and sample preparation. *Frontier Research on Earth Evolution*, 2, 1–8.
- Taylor, B. (1992). Rifting and the volcanic-tectonic evolution of the Izu-Bonin-Mariana arc. In B. Taylor, K. Fujioka, (Eds.), *Proceedings of the Ocean Drilling Program, Scientific Results 126* (pp. 627–651). College Station, TX: Ocean Drilling Program.
- Taylor, R. N., & Nesbitt, R. W. (1998). Isotopic characteristics of subduction fluids in an intra-oceanic setting, Izu-Bonin Arc, Japan. *Earth and Planetary Science Letters*, 164, 79–98.
- Tollstrup, D., Gill, J., Kent, A., Prinkey, D., Williams, R., Tamura, Y., & Ishizuka, O. (2010). Across-arc geochemical trends in the Izu-Bonin arc: Contributions from the subducting slab, revisited. *Geochemistry, Geophysics, Geosystems*, 11, Q01X10. <https://doi.org/10.1029/2009GC002847>
- Yamashita, M., Takahashi, N., Tamura, Y., Miura, S., & Kodaira, S. (2018). Seismic imaging for an ocean drilling site survey and its verification in the Izu rear arc. *Exploration Geophysics*, 49(1), 1–10. <https://doi.org/10.1071/EG16142>
- Yamazaki, T., & Yuasa, M. (1998). Possible Miocene rifting of the Izu-Ogasawara (Bonin) arc deduced from magnetic anomalies. *Island Arc*, 7, 374–382.

How to cite this article: Sato T, Miyazaki T, Tamura Y, et al.

The earliest stage of Izu rear-arc volcanism revealed by drilling at Site U1437, International Ocean Discovery Program Expedition 350. *Island Arc*. 2020;e12340. <https://doi.org/10.1111/iar.12340>